Eur. Phys. J. A **30**, 71–79 (2006)
DOI 10.1140/epja/i2006-10108-7

THE EUROPEAN PHYSICAL JOURNAL A

Systematics of fragment observables

B. Tamain[a]

LPC Caen (IN2P3-CNRS/Ensicaen et Université), F-14050 Caen Cédex, France

Received: 25 April 2006 /
Published online: 19 October 2006 –

Abstract. Multifragmentation is observed in many reaction types: light-ion–induced reactions at large incident energies (in the GeV region), central heavy-ion collisions from 30 to 100 MeV/u, and peripheral heavy-ion collisions between 30 and 1000 MeV/u or above. When nucleus-nucleus collisions are considered, another entrance channel parameter is the corresponding mass asymmetry. The first question which is addressed in this contribution is: do we observe similar reactions in each case? Multifragmentation may be related to a phase transition of nuclear matter. Some others features indicate that dynamical features are dominant. It is *a priori* possible that the underlying mechanisms are different in proton- and nucleus-induced reactions, in central and in peripheral collisions, at limited and at large bombarding energies. In order to see to what extent they can reflect similar behaviour, it is useful to compare the results of various reactions. The observables can be the fragment multiplicity, the mass distributions or the kinematical properties. In this contribution, we are looking for such general features. We will limit the discussion to the observations themselves, rather than the interpretation, which is the subject of numerous entries in this volume. The experimental results indicate that multifragmentation exhibits at the same time universal and entrance-channel–dependent properties.

PACS. 24.10.Pa Thermal and statistical models – 25.70.Pq Multifragment emission and correlations – 68.35.Rh Phase transitions and critical phenomena

1 The necessity and the difficulty of the sorting

A first difficulty in comparing nucleus-nucleus collision data lies in the fact that they can differ significantly according to the impact parameter. Now, the impact parameter cannot be directly measured: it can be only estimated from other more direct observables. Depending on the experiment, various sorting parameters have been used: neutron or light charged particle (LCP) or total charged particle multiplicity [1–4], or LCP (or total) transverse energy [5], or flow angle [6], or specific quantities like *Erat* (ratio between the total perpendicular and parallel kinetic energy) [7] or Z_{bound} (the total charge bound in fragments) [8,9]. One may also use more sophisticated methods as the principal component analysis method [10] or calorimetry [11,12] (see also the contribution V.3 in this topical issue [13]).

The sorting aims either at following the evolution of the mechanism when the violence of the collision is increased (from peripheral to central collisions for nucleus-nucleus collisions), or at selecting something which is generally labelled "a source". An example is the selection of central collisions in nucleus-nucleus collisions. In the previous sentences, we have two concepts: "the collision violence" and "the source".

The violence is linked with the proportion of the initial aligned energy (the kinetic energy of the beam) that is shared among other degrees of freedom. It may be linked with a thermal energy if the available phase space is fully explored for the ensemble of selected events. A "source" is a piece of nuclear matter that is localized in momentum space. It is not necessarily equilibrated.

An important question is the quality of the sorting: to what extent is the selection efficient? The sorting cannot be precise for several reasons: finite-size effects; detection inefficiency (dead areas and thresholds); fluctuations in the energy sharing in multi-source processes (for instance, in binary processes). One may have an idea of this precision by looking at the correlation between various sorting variables. Data have been obtained for instance at MSU [1] in which particle multiplicities and transverse energies have been correlated. Another example has been obtained by the INDRA-ALADIN Collaboration [14]: in this case, binary symmetrical collisions have been studied and transverse energy correlations have been obtained between the projectile-like (PLS) and the target-like (TLS) sources. The correspondences are not better than about 20 percent. This means that for a selected value of a selected sorting variable, the variation range of a second sorting

[a] e-mail: tamain@in2p3.fr

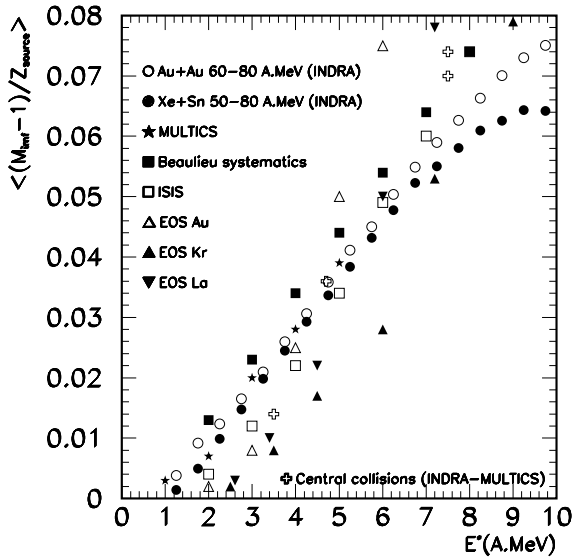

Fig. 1. Correlation between $(M_{IMF} - 1)/Z_{source}$ (ordinate) and the dissipated energy (abscissa). The excitation (dissipated) energy has been corrected for pre-equilibrium and for expansion (if any: it is especially the case for the EOS data [4]). In that sense, the dissipated energy is mainly thermal. Several systems have been "summarized" in a single data set when the results were very close: it is the case for the Laval and ALADIN data [11] and for the INDRA@GSI data [15]. Other data are extracted from refs. [2,10,16,17]. This figure has been prepared with the help of R. Bougault.

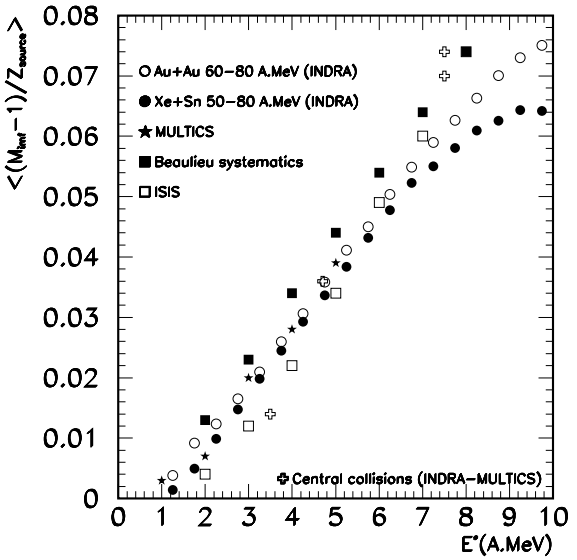

Fig. 2. This figure is similar to the previous one but the EOS data have been removed. It turns out that the coherence between various reactions is very good in spite of the fact that one has included in the figure peripheral and central collisions, light- and heavy-nucleus–induced rections.

variable covers about 20 percent of its mean value: sorting is efficient but not very precise. In any case, the detection has to be as complete as possible. It is possible to study the continuous evolution of the sorting variable keeping in mind that some mixing cannot be avoided. It is difficult to isolate a definite class of events without encountering one or another drawback: either a mixing with other event classes; or a cut in the available phase space for the selected event class. This difficulty is very well understood in simulations. Sorting from a mixing of various variables (principal component analysis) can slightly improve the quality of the selection [10,18,19].

2 Fragment observables

The raw multifragmentation observables are multiplicities, mass or charge distributions, isotopic distributions, kinetic energy and angular distributions. They can have various meanings depending on the collision nature: nucleus-nucleus collision *versus* light-projectile (p, d, α, $\bar{p}$, π) induced reactions; peripheral *versus* central collisions.

Various observables can also magnify different collision features. This can be illustrated from what is well known at low bombarding energies, below 10 MeV/u. In this case, deep inelastic reactions are dominant and it is well known that, depending on the observable, one is focussing on various aspects of the collision: fragment angular and kinetic energy distributions (Wilczynski plots) reflect the dynamics of the process: complete damping and isotropy is not observed for most of the events. On the other hand, mass transfer is described with Fokker-Planck equations for which some degrees of freedom (the fast ones) are thermally treated (heat bath) whereas some others (mass transfer) are slowly evolving and do not reach necessarily equilibrium.

3 Fragment production: a hierarchy

At low bombarding energy, it is well known that the decay of an excited nucleus ends with residue production. This decay product has a specific role among all the disentegration products. This feature is clear at low energy. A recent compilation [20] and the results of figs. 1 and 2 indicate that this specific role of the largest fragment is often evidenced. It is the reason why, in the next sections, one will distinguish the largest fragment from the others.

4 Fragment production: multiplicities

We label "fragments" as the detected products with an atomic number Z of at least 3, which are generally named intermediate mass fragments (IMF). The lighter products (Z smaller than 3) are labelled light charged particles (LCP). The fragment multiplicity is M_{IMF}.

To what extent is M_{IMF} correlated with energy dissipation? At low bombarding energies, it is established that $M_{IMF} - 1$ is close to zero since no IMFs are emitted other than the residue: only LPCs remove the deposited energy. The situation is more complicated for larger energy deposition for which the pre-equilibrium energy contribution is significant and not uniquely defined. It has

Table 1. This table is a non-exhaustive compilation of many experiments in which the IMF multiplicities have been measured as a function of the excitation (dissipated) energy. The systems involved are indicated in the first column. The projectiles can be light (pions) or heavy (up to gold nuclei); the selected collisions can be central (one single source), or peripheral (projectile-like source). The references are also indicated in the first column. The second column indicates the method that has been used to determine the excitation energy given in the fourth column. Two excitation energies have been selected: around 4 MeV and aroud 8 MeV/u, corresponding to close to and above the multifragmentation threshold. The fragment multiplicities (except for the heaviest fragment) normalized to the source size are given in the last column.

System	Method	Z_{source}	E^*/u (MeV)	$(M_{IMF}-1)/Z_{source}$
π + Au 8 GeV/c; [11]	cal	67	4	0.022
Cl + Au 43 MeV/u; peripheral; [21]	cal	17	4	0.035
Ge + Ti 35 MeV/u; peripheral; [21]	cal	32	4	0.035
Nb + Mg 30 MeV/u; central; [16]	cal	45	3.4–3.8	0.014
Au + Au 35 MeV/u; peripheral; [2]	cal	≈ 75	4	0.030
Au + Au 600 MeV/u; peripheral; [9]	cal	≈ 75	4	0.035
System	Method	Z_{source}	E^*/u (MeV)	$(M_{IMF}-1)/Z_{source}$
π + Au 8 GeV/c; [11]	cal	59	7–8	0.068
Cl + Au 43 MeV/u; peripheral; [21]	cal	17	8	0.071
Ge + Ti 35 MeV/u; peripheral; [21]	cal	32	8	0.071
Ni + Au 90 MeV/u; central; [10]	cal/SMM	86	7.5	0.070
Xe + Sn 50 MeV/u; central; [10]	cal/SMM	85	7–8	0.074
Xe + Sn 80 MeV/u; peripheral; [15]	cal	48	8	0.077
Au + Au 80 MeV/u; peripheral; [15]	cal	70	7	0.069
Au + Au 600 MeV/u; peripheral; [9]	cal	55	8	0.073
Au + C 1000 MeV/u; semi-peripheral; [4]	cal	53–40	7.5	0.10
La + C 1000 MeV/u; semi-peripheral; [4]	cal	40–34	7.5	0.077
Kr + C 1000 MeV/u; semi-peripheral; [4]	cal	26–23	7.5	0.07

to be subtracted. After this subtraction, excitation energy is usually measured by calorimetry. It can be also obtained from the comparison with a model (for instance, SMM [22]) in which equilibrium is assumed. When the bombarding energy is large, some compression effect may also be present and the corresponding expansion energy can be taken away. All these procedures can be disputed. Nevertheless, we have compared many data obtained in various ways to try to evidence some general behaviours. In table 1, such a compilation is shown for two values of the "measured" excitation energy: 4 MeV/u and 8 MeV/u. The list is not exhaustive. Since the expansion energy has been subtracted, the word "thermal" energy could be more appropriate but its use can be considered as too precise. For this reason, we will use the word "dissipated" for which the consensus may be better obtained. Very different reaction types are considered in table 1: pion-induced reactions, central or peripheral heavy-ion reactions, intermediate (35 MeV/u) or large (1000 MeV/u) bombarding energies. The method used to estimate the excitation energy can be calorimetry or comparison with SMM (indicated in the second column). The source size Z_{source} is also estimated in various ways [23]. Nevertheless, it appears that the ratio $(M_{IMF}-1)/Z_{source}$ seems to be about the same for a defined excitation energy. This result is a first indication that multiframent production could be correlated with the dissipated energy.

This tendency is confirmed from figs. 1 and 2 which show the correlation between $(M_{IMF}-1)/Z_{source}$ and the measured excitation (dissipated) energy. All the systems considered in table 1 have been used. In order to clarify the figure, several systems are sometimes "summarized" by a single result. This is the case for the INDRA@GSI data or for the Laval + ALADIN data [21]. The general tendency is again the same for any system whatever the entrance channel is: light or heavy projectile; low or large incident energy; central or peripheral collisions (see also ref. [24]). The coherence is especially good for high excitation (dissipation) energy and in fig. 2 in which the EOS data have not been included. The fact that the EOS data do not fit so well with others can be understood since in this case, the non-thermal contributions which are subtracted are huge and difficult to estimate with a good precision.

The results plotted in figs. 1 and 2 indicate a continuous increase of the ordinate. One knows also that at larger dissipations, the fragment multiplicities decrease: *i.e.* the rise and fall of multifragment emission [4,8] for which a universal behaviour is also established (see figs. 3 and 4). Altogether, there is a continuous evolution from low-energy collisions with a large released residue to complete vaporization with only LCPs. The specific role of the largest fragment is evident at low exitation and disappears when complete vaporization sets in; in between, the meaning of the fragment hierarchy is still open to debate and is interpreted either as a dynamical effect reflecting the

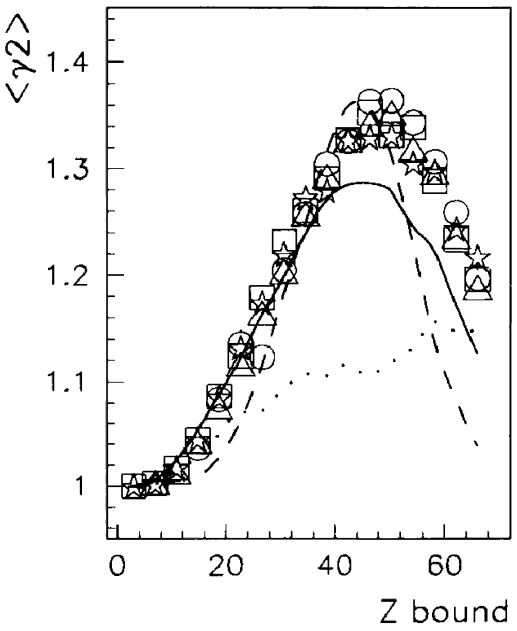

Fig. 3. Rise and fall of the fragment multiplicity as a function of the total detected bound charge which is expected to be related to the dissipated energy. Different symbols correspond to PLS sources produced in Au collisions on different targets ranging from C to Pb. Extracted from ref. [8].

collision geometry, or in terms of liquid-gas coexistence. Further experimental and calculation results are needed in order to progress on this point.

Fragment multiplicities are in any case correlated with the energy dissipated in the collision. This property has sometimes been described in terms of reducibility [5,25] in the sense that the probability for emitting several fragments can be reduced to the probability for emitting a single fragment and to the corresponding energy cost. Such a result is quite coherent with the above discussion of figs. 1 and 2.

Thus it seems that multifragment production is to a large extent defined by the energy dissipated during the collision. Of course, the correlation obtained from the data cannot be perfect for two reasons. First of all, it is impossible to measure properly the "dissipated" energy because it is not possible to separate clearly in the data the relative contributions of pre-equilibrium, compression or thermal parts. A second feature is that many aspects of the collisions reflect an important role of the dynamics which is observed in mid-rapidity and in forward-backward emissions. These contributions are to a large extent responsible for the deviations observed between the data at low dissipations in figs. 1 and 2. They are discussed in the next section.

5 Pre-equilibrium emissions

5.1 General observations

Pre-equilibrium emissions correspond to particles or fragments that are not randomly emitted from identified

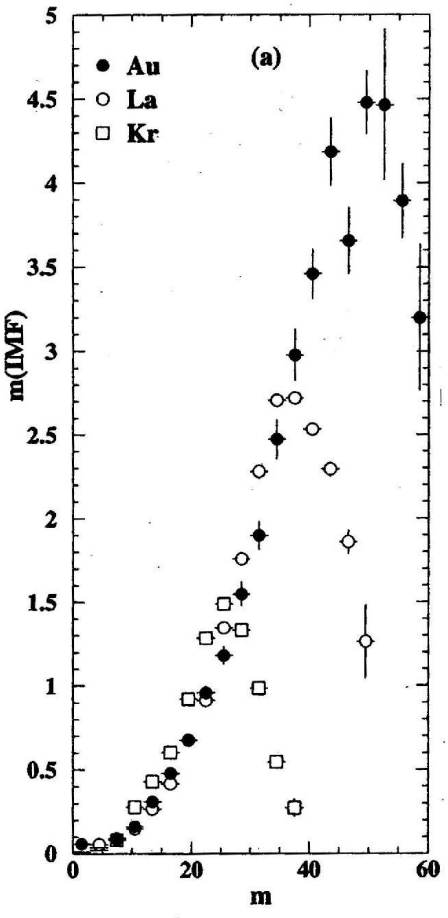

Fig. 4. Rise and fall of the fragment multiplicity as a function of the total particle multiplicity which is correlated with the energy dissipated in the PLS released in several nucleus-nucleus collisions for various systems. Extracted from ref. [4]

sources (no isotropic emission in the plane perpendicular to the angular momentum). Besides the key quantities such as energy and angular momentum, they have kept some memory of the entrance channel, *i.e.* of the beam direction and/or velocity. From the time scale point of view, pre-equilibrium particles are emitted early. Their center-of-mass kinetic energies are generally larger than expected after full equilibrium, reflecting the fact that the incident beam energy has not been shared among all the available degrees of freedom. The energy relaxation step brings energy in various degrees of freedom: the stored energy can be thermal if the whole available phase space has been occupied. The energy can also partially be stored as compression energy of nuclear matter, thus leading to an additional expansion contribution. A fraction of the available energy can also be stored as deformation energy of the hot source. The distinction between pre-equilibrium, expansion and thermal contributions is not trivial since the mean thermal decay time becomes very short for large excitations.

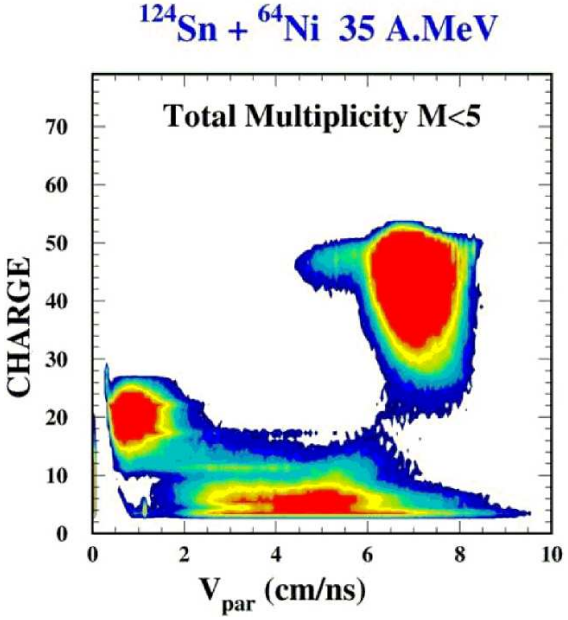

Fig. 5. Correlation between the charges and the velocities of products emitted in semi-peripheral nucleus-nucleus collisions. Mid-rapidity is evidenced for light IMFs. Similar results are published in ref. [26].

5.2 Angular distributions as signatures of pre-equilibrium

Two kinds of pre-equilibrium emissions are recognized in the data. In particle-nucleus or in central nucleus-nucleus collisions, pre-equilibrium LCP angular distributions are mostly forward or backward peaked relative to the beam direction.

In semi-peripheral reactions, mid-rapidity neck emission occurs both for LCP and IMF. Pre-equilibrium LCPs result mainly from direct nucleon-nucleon collisions in the overlap zone (see sect. 5.3). Concerning fragments, a general observation is that the largest decay fragment from a projectile-like source (PLS) is mostly faster than the lighter IMFs that are detected forward in the c.m. frame [26–28]: these lighter IMFs are accumulated close to the backward part of the Coulomb ring associated to the PLS whatever the bombarding energy is [29]. If the incident energy is limited (40 MeV/u or below), this backward part of the Coulomb ring is close to the c.m. velocity (mid-rapidity). The data of fig. 5 correspond to this situation. Neck emission is clearly an entrance dynamical effect that leads to ambiguities in the measurement of the dissipated energy in a projectile-like source. It affects the projectile-like source velocity if it is reconstructed from the detected fragments. It affects also the excitation energy calculated from calorimetry. This ambiguity is larger when neck contribution is a sizeable fraction of the whole total yield. This is especially true for limited excitations and for symmetric heavy-ion collisions [30]. This can explain partially the relative dispersion of data in figs. 1 and 2 at limited dissipations.

Depending on the observable, one may focus more or less on dynamical features. Neck emission is used in this context. On the contrary, one may subtract identified pre-equilibrium particles to try to isolate sources and try to get their excitation energies. Finally, one may select events for which the pre-equilibrium energy is small and can be neglected [2,23]. This procedure is never perfect especially for symmetric collisions in the entrance channel. Nevertheless, it is possible to isolate events for which most of the available energy has been shared among many degrees of freedom. The deviations from full exploration of the available phase space can be to some extent "summarized" in collective variables such as deformation or expansion, which can be associated to Lagrange parameters [31].

The fact that the results of figs. 1 and 2 are coherent indicate that extracting dissipated energies from the data is a meaningful procedure. Similarly, we will see in sect. 6 that the released IMF observables indicate that the process reflects to a large extent the available phase space.

5.3 Kinetic energies as signatures of pre-equilibrium

Another indication of pre-equilibrium can be found in the measured kinetic energies of the emitted LCP and IMF. In semi-peripheral collisions, entrance channel effects are clearly evidenced [32,33]. For instance, in ref. [32], it is shown that the transverse LCP energy at mid-rapidity does not depend on the violence of the collision at variance with the energy of LCP emitted from the PLS (fig. 6). LCPs emitted at mid-rapidity reflect the incident energy per nucleon and the Fermi motion of the projectile and target nucleons whereas LCPs emitted at velocity closer to the PLS one reflect the dissipated energy. Depending

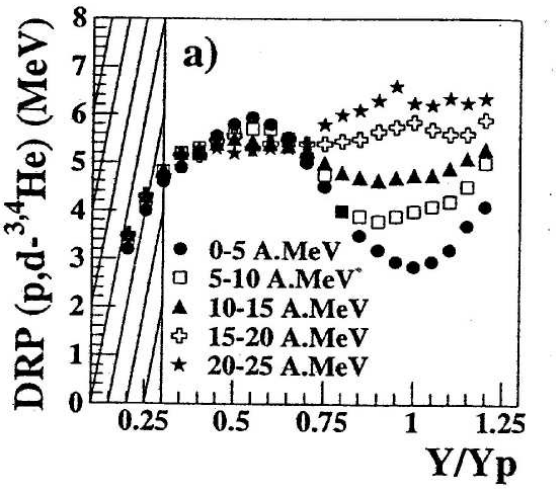

Fig. 6. Abscissa: rapidity of selected LCPs in beam rapidity units; ordinate: double ratio parameter (p, d, He thermometer) corresponding to the abscissa rapidity. Various curves correspond to various energy dissipations (the excitation energy per nucleon has been measured by calorimetry in assuming a binary reaction: see ref. [32] for details). The dissipated energy has no influence on the results obtained at mid-rapidity.

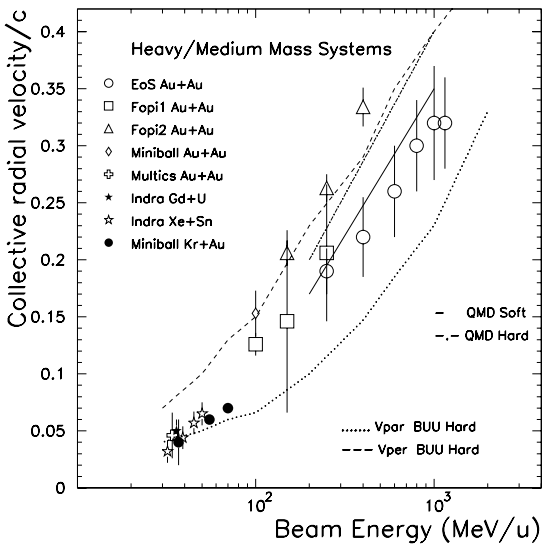

Fig. 7. Non-exhaustive compilation for the collective radial velocity as a function of the beam energy for medium- and heavy-mass systems in central collisions. Lines correspond to the predictions of transport models; for BUU calculations, the collective motion is found to be anisotropic so that both v_{par} and v_{perp} are shown. From ref. [34] and references therein.

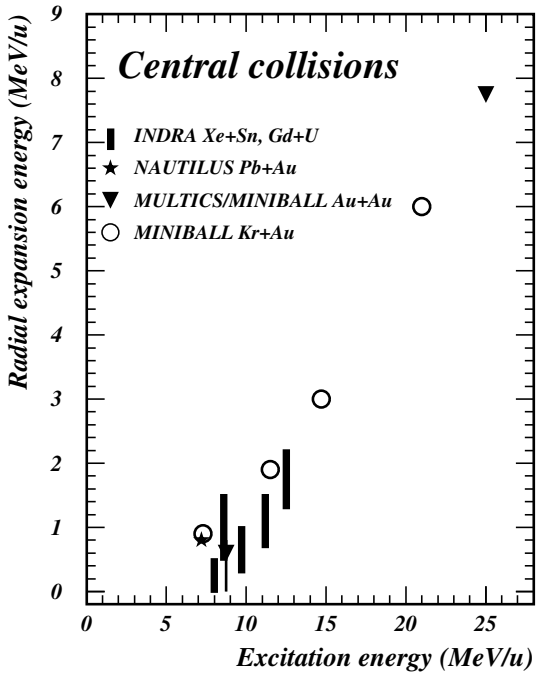

Fig. 8. Systematics of the collective expansion energy as a function of the available center-of-mass energy per nucleon in central collisions [35].

on the location in the velocity plane, we observe entrance channel or dissipation effects.

In central collisions, the LCP kinetic energy spectra exhibit non-Maxwellian shapes especially along the beam direction. Many data have been interpreted in unfolding the measured spectra in order to separate two components: pre-equilibrium on the one side and an equilibrated part on the other side. Their relative contributions depend strongly on the emission angle which is a help to succeed in the unfolding. For the equilibrated part, the mean c.m. kinetic energy $\langle\epsilon\rangle$ depends on the mass of emitted LCP or IMF. This result indicates that a non-thermal component is present. It is generally attributed to an expansion energy reflecting nuclear-matter compression properties. Figure 7 is a non-exhaustive compilation showing that expansion energy (or radial velocity) is small for incident energies lower than 30 MeV/u [34]. Conversely, fig. 8 indicates that expansion is significant for measured excitation (deposited) energies exceeding 5 to 6 MeV/u [35].

6 Charge or mass distributions

We have already noticed in sect. 3 that the heaviest fragment emitted from a selected source plays a significant role among all the outgoing fragments. This is the case at excitation energies below the multifragmentation threshold since, in this case, the largest fragment is an evaporation residue. When multifragmentation occurs, the largest fragment has no longer this specific role and its mass becomes much lower. It is observed in the experiments that this change from evaporation-like events to multifragmentation is rather abrupt when the dissipation is increased. In some cases, the coexistence of evaporation-like and multifragmentation events has been observed for comparable dissipations: it is the bimodality signal that is a possible signature of a phase transition of the system (see O. Lopez and M.F. Rivet, this topical issue). It is only stressed here that bimodality can be a first indication of a statistical behaviour for defining the masses or charges of the products released in nucleus-nucleus collisions.

More generally speaking, many data indicate that the overall charge and mass distributions can be described by statistical models, *i.e.* in models in which the main ingredient is the available phase space. This is true for the total charge distribution [2,23] and for the distributions associated with the largest or the second and third largest fragment [18,17]. This is true for limited excitations [2] for which few fragments are released up to very large ones leading to vaporization [36]. In this last case, only LCP are detected but their relative abundances are also understood in a statistical approach [37]. An interesting compilation is shown in fig. 9. It concerns several experiments with quite different entrance channels and for which the measured mass distributions seem to reflect mainly the deposited energy in MeV/u. Similarly, it has been shown in ref. [2] that similar results are found in peripheral and central collisions, indicating that the dissipated energy seems again to be the main ingredient which defines the splitting of the system.

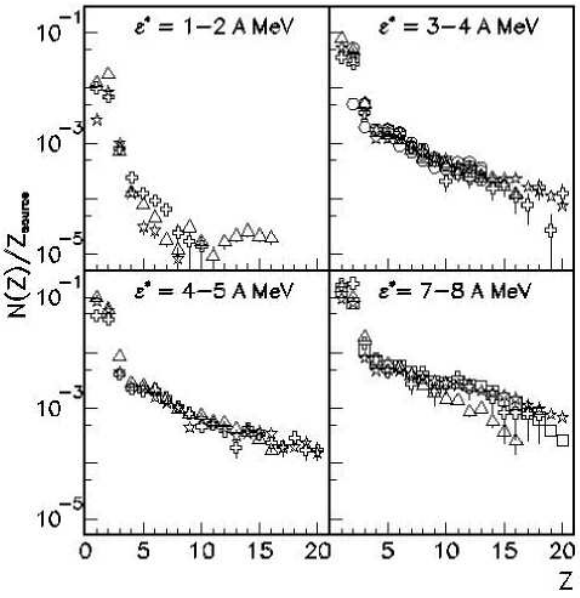

Fig. 9. Mass distribution for various excitation energy ranges obtained in several experiments involving very different entrance channels: stars: Au + Au central collisions from MULTICS data [2]; crosses: peripheral collisions with MULTICS [17]; hexagons: FASA data [38]; squares: 32 MeV/u Xe + Sn INDRA data [10]; triangles: ISIS data [11]. This figure has been prepared by M. D'Agostino [39,40].

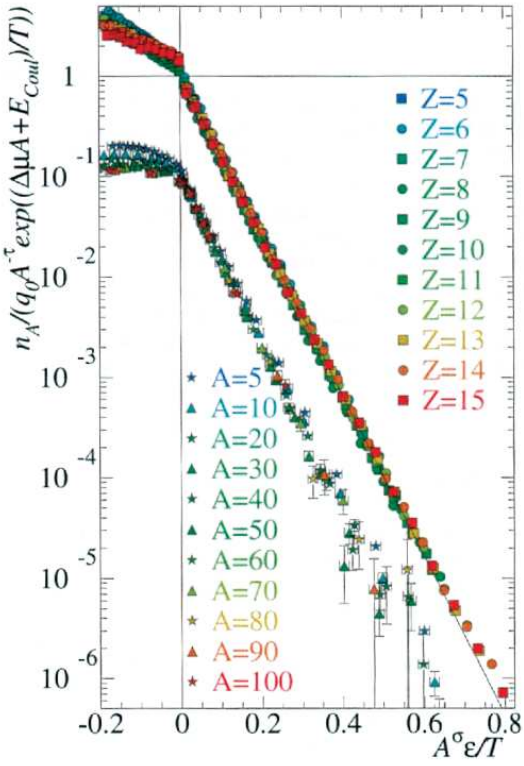

Fig. 10. Analysis of the ISIS data showing that the probability for emitting a given fragment can be fitted in the Fisher formalism in which the emission is mainly governed by statistical properties of nuclei [44].

Many results are reproduced by models like SMM [22] or MMMC [41] in which full statistical equilibrium is assumed. Of course, one may argue that such agreements can be obtained only by adjusting parameters such as the density at freeze-out. The total mass and the excitation energy of the initial source are also adjusted to reproduce the data, but their values are in agreement with calorimetric measurements when they are available. The excitation energies and source masses are smaller than the available energy and mass simply because of pre-equilibrium emission. More direct data are also available in which several systems are compared independently of a model. For instance, in ref. [42] it is shown that the systems Xe + Sn and Gd + U exhibit similar mass distributions at similar measured excitation energies in MeV/nucleon. Similarly, in ref. [10], central Xe + Sn and Ni + Au collisions (same fusion-like source mass at similar excitation energies) exhibit similar mass distributions. This dominance of phase space is also evidenced by the fact that the observed multifragmentation mass distributions can be reproduced simply in cutting at random a rope in a number of elements equal to the observed multiplicity [43]. The multifragmentation mass distribution would hence be constrained only by the mass conservation for a given fragment multiplicity.

One of the most spectacular results indicating a statistical behaviour is the reducibility property [25] which indicates that fragment production probabilities can be put together in Arrhenius plots and the very beautiful fits obtained in the so-called scaling analysis. Figure 10 is the most famous one but similar fits have been obtained with other data [2,45]. Even if such an analysis relies on several adjusted parameters (which are consistent with theoretical expectations) and in spite of the blurring effects of secondary decay, this property is a further evidence of statistical behaviour.

An isospin analysis of the released products is also in agreement with this statement [18,46,47]: isoscaling is the observation that the probability ratio for producing a defined isotope in two different reactions may be expressed as:

$$R_{1,2} = \exp(\alpha N + \beta Z), \quad (1)$$

where N and Z are the neutron and proton numbers of the isotope. Even if the physics is not transparent for the values of the parameters α and β [28], the validity of eq. (1) indicates that statistical features are present everywhere. Figure 11 is an illustration showing that this description is valid over a wide range of incident energies and reactions. In this figure, $R_{1,2}$ has been multiplied by $\exp(\beta Z)$ in order to express the results only as a function of N. Scaling is observed for deep inelastic collisions, for evaporation and for multifragmentation as well. It is consistent with the fact that all these processes are governed by the available final states [48]. It does not seem that the sequential decay affects significantly the results [49]. Nevertheless, such observations do not mean that full equilibrium is achieved and some FOPI data [7] indicate that the full mixing be-

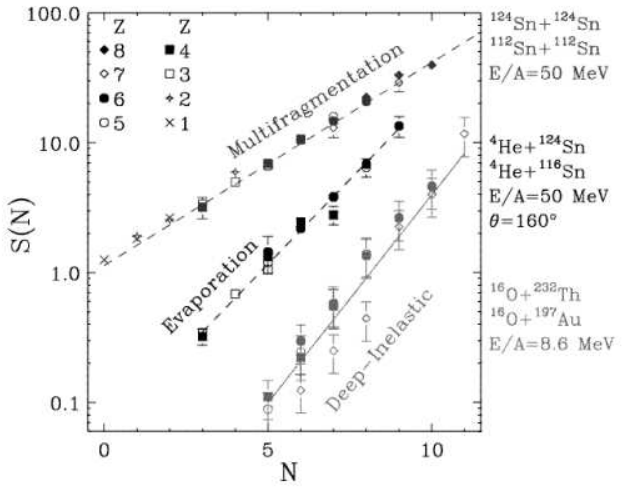

Fig. 11. Production ratio for various isotopes and several reaction pairs. The isoscaling as a function of the neutron number is observed for very different reaction types, from evaporation and deep inelastic collisions to multifragmentation. See text for details. Extracted from ref. [46].

tween the projectile and the target is not achieved even in the most central collisions. Hence, the available phase space is widely opened but is still constrained by some entrance channel memory.

7 Conclusion

From many data, fragment production exhibits both dynamical and statistical aspects. The multiplicity is mainly governed by the dissipated energy. It increases from a single residue (or two fission fragments) for limited excitations up to large values in the multifragmentation regime, the rise and fall leading to a vanishing multiplicity when the dissipated energy is sufficient to allow vaporization. In the multifragmentation case, some fragments can be released in dynamical processes such as neck emission observed in semi-peripheral collisions. In any case, fragments are accompagnied by multiple light particles, some of which show dynamical features.

The size distributions of the detected fragments are also mainly governed by the available phase space; the heaviest fragment has specific properties at least for limited excitations, below 3–5 MeV/u, *i.e.* below the threshold energy for which the multifragmentation channel sets in significantly. Above this threshold, the specificity of the heaviest fragment is weaker.

However, many kinematical properties of the fragments reflect dynamics in the sense that they have retained some memory of the entrance channel. This is clearly the case for their angular distributions and also for their kinetic energies which are not purely thermal for nucleus-nucleus collisions at bombarding energies exceeding 50 MeV/u even if central collisions are selected. This deviation from a thermal behaviour can sometimes be interpreted as a collective deformation [50] or compression effect initiated by the early compression phase in the collision. In such a case, a statistical description can be used provided that one introduces in the description a constraint summarizing the dynamical behaviour.

References

1. L. Phair *et al.*, Nucl. Phys. A **548**, 489 (1992).
2. MULTICS Collaboration (M. D'Agostino *et al.*), Nucl. Phys. A **724**, 455 (2003).
3. R. Wada *et al.*, Phys. Rev. C **69**, 044610 (2004).
4. EOS Collaboration (L. Hauger *et al.*), Phys. Rev. C **62**, 024616 (2000).
5. L. Moretto *et al.*, Phys. Rev. Lett. **74**, 1530 (1995).
6. INDRA Collaboration (J. Frankland *et al.*), Nucl. Phys. A **689**, 905 (2001).
7. FOPI Collaboration (F. Rami *et al.*), Phys. Rev. Lett. **84**, 1120 (2000).
8. ALADIN Collaboration (P. Kreutz *et al.*), Nucl. Phys. A **556**, 672 (1993).
9. ALADIN Collaboration (W. Trautmann *et al.*), in *Proceedings of the XXXIII International Winter Meeting on Nuclear Physics, Bormio, Italy, 1995*, edited by by I. Iori, Suppl. # 101 (Ricerca Scientifica ed Educazione Permanente, Milano, 1995) p. 372.
10. INDRA Collaboration (N. Bellaize *et al.*), Nucl. Phys. A **709**, 367 (2002).
11. L. Beaulieu *et al.*, Phys. Rev. C **64**, 064604 (2001).
12. Y.G. Ma *et al.*, Phys. Rev. C **69**, 031604 (2004).
13. V.E. Viola, R. Bougault, contribution V.3, this topical issue.
14. M. Pichon *et al.*, unpublished data.
15. INDRA-ALADIN Collaboration, unpublished results.
16. L. Manduci, PhD Thesis, Caen, 2005.
17. M. D'Agostino *et al.*, Nucl. Phys. A **650**, 329 (1999).
18. CHIMERA Collaboration (E. Geraci *et al.*), Nucl. Phys. A **734**, 524 (2004).
19. INDRA Collaboration (P. Lautesse *et al.*), Phys. Rev. C **71**, 034602 (2005).
20. R. Bougault *et al.*, to be published.
21. L. Beaulieu *et al.*, Phys. Rev. C **54**, R973 (1996).
22. J. Bondorf *et al.*, Phys. Rep. **257**, 133 (1995).
23. INDRA Collaboration (N. Marie *et al.*), Phys. Lett. B **391**, 15 (1997); Phys. Rev. C **58**, 256 (1998).
24. INDRA Collaboration (V. Metivier *et al.*), Nucl. Phys. A **672**, 357 (2000).
25. L. Moretto *et al.*, Phys. Rep. **287**, 249 (1997).
26. A. Pagano *et al.*, Nucl. Phys. A **734**, 504 (2004).
27. INDRA Collaboration (J. Colin *et al.*), Phys. Rev. C **67**, 064603 (2003).
28. S.R. Souza *et al.*, Phys. Rev. C **69**, 031607R (2004).
29. INDRA-ALADIN Collaboration (J. Łukasik *et al.*), Phys. Lett. B **566**, 76 (2003).
30. INDRA Collaboration (F. Bocage *et al.*), Nucl. Phys. A **676**, 391 (2000).
31. P. Chomaz *et al.*, Ann. Phys. **320**, 135 (2005).
32. T. Lefort *et al.*, Nucl. Phys. A **662**, 397 (2000).
33. INDRA-ALADIN Collaboration (J. Łukasik *et al.*), Phys. Rev. C **66**, 064606 (2002).
34. D. Durand, Nucl. Phys. A **654**, 273c (1999); D. Durand *et al.*, *Nuclear Dynamics in the Nucleonic Regime* (IOP Publishing Ltd, 2001).

35. M.F. Rivet *et al.*, *Proceedings of the XXVII International Workshop on Gross Properties of Nuclei and Nuclear Excitations, Hirschegg, Austria, 1999*, edited by H. Feldmeier *et al.* (GSI, Darmstadt, 1999) p. 293.
36. INDRA Collaboration (M.F. Rivet *et al.*), Phys. Lett. B **388**, 219 (1996).
37. INDRA Collaboration (B. Borderie *et al.*), Eur. Phys. J. A **6**, 197 (1999).
38. FASA Collaboration (V.A. Karnaukhov *et al.*), Nucl. Phys. A **734** 520 (2004).
39. M. D'Agostino *et al.*, Nucl. Phys. A **749**, 55 (2005).
40. M. D'Agostino, unpublished.
41. D.H.E. Gross, Rep. Prog. Phys. **53**, 605 (1990).
42. INDRA Collaboration (M.F. Rivet *et al.*), Phys. Lett. B **430**, 217 (1998); INDRA Collaboration (J. Frankland *et al.*), Nucl. Phys. A **689**, 940 (2001).
43. R. Dayras, unpublished calculations.
44. J.B. Elliott *et al.*, Phys. Rev. Lett. **88**, 042701 (2002).
45. INDRA Collaboration (N. Leneindre), submitted to Eur. Phys. J. A.
46. M.B. Tsang *et al.*, Phys. Rev. Lett. **86**, 5023 (2001).
47. G.A. Souliotis *et al.*, Phys. Rev. C **68**, 024605 (2003).
48. D.V. Shetty *et al.*, Phys. Rev. C **71**, 024602 (2005).
49. M.B. Tsang *et al.*, Phys. Rev. C **64**, 054615 (2001).
50. INDRA-ALADIN Collaboration (A. Lefèvre *et al.*), Nucl. Phys. A **735**, 219 (2004).